Local Protein Dynamics and Catalysis: Detection of Segmental Motion Associated with Rate-Limiting Product Release by a Glutathione Transferase†

Simona G. Codreanu,‡ Jane E. Ladner,§ Gaoyi Xiao,§ Nina V. Stourman,‡ David L. Hachey,‡ Gary L. Gilliland,§ and Richard N. Armstrong*,‡

Departments of Chemistry and Biochemistry, Center in Molecular Toxicology, Vanderbilt University School of Medicine, Nashville, Tennessee 37232-0146, and Center for Advanced Research in Biotechnology, Maryland Biotechnology Institute, University of Maryland, Shady Grove, and National Institute of Standards and Technology, 9600 Gudelsky Drive, Rockville, Maryland 20850

Received September 3, 2002; Revised Manuscript Received October 23, 2002

ABSTRACT: Glutathione transferase rGSTM1-1 catalyzes the addition of glutathione (GSH) to 1-chloro-2,4-dinitrobenzene, a reaction in which the chemical step is 60-fold faster than the physical step of product release. The hydroxyl group of Y115, located in the active site access channel, controls the egress of product from the active site. The Y115F mutant enzyme has a k_{cat} (72 s^{-1}) that is 3.6-fold larger than that of the native enzyme (20 s^{-1}). Crystallographic observations and evidence from amide proton exchange kinetics are consistent with localized increases in the degree of segmental motion of the Y115F mutant that are coupled to the enhanced rate of product release. The loss of hydrogen bonding interactions involving the hydroxyl group of Y115 is reflected in subtle alterations in the backbone position, an increase in *B*-factors for structural elements that comprise the channel to the active site, and, most dramatically, a loss of well-defined electron density near the site of mutation. The kinetics of amide proton exchange are also enhanced by a factor between 3 and 12 in these regions, providing direct, quantitative evidence for changes in local protein dynamics affecting product release. The enhanced product release rate is proposed to derive from a small shift in the equilibrium population of protein conformers that permit egress of the product from the active site.

The glutathione transferases (EC 2.5.1.18) catalyze the addition of glutathione (GSH)[1] to both endogenous and xenobiotic electrophilic compounds. They are perhaps the single most important group of enzymes for initiating the metabolism and disposition of potentially toxic alkylating agents. The canonical GSH transferase superfamily consists of at least nine subfamilies (*1*, *2*). The structural and functional aspects of these dimeric enzymes have been studied extensively over the past three decades. A historical perspective and recent reviews are available (*2*−*6*). Crystallographic studies reveal that the subunit polypeptide is organized into two domains, a GSH binding domain (domain I) at the N-terminus and a xenobiotic substrate binding domain (domain II) at the C-terminus (*7*, *8*).

The enzymes exhibit a remarkable degree of catalytic diversity with single isoenzymes catalyzing multiple reaction types. The extent and type of participation of individual residues in catalysis are highly dependent on the nature of the transition state and the rate-limiting step for the reaction in question. Some years ago, we presented mechanistic and structural evidence that Y115, located in domain II of a rat class mu enzyme (rGSTM1-1), played distinctly different roles in the addition of GSH to epoxides and in nucleophilic aromatic substitution (S_NAr) reactions (*9*). The hydroxyl group of Y115 provides electrophilic assistance in the addition of GSH to an arene oxide substrate, a reaction in which the chemical step is rate-limiting (Figure 1A). In contrast, the same hydroxyl group was proposed to control the egress of product from the active site in the addition of GSH to 1-chloro-2,4-dinitrobenzene, a reaction in which product release is the rate-limiting step in turnover (Figure 1B). The removal of the hydroxyl group in the Y115F mutant has quite different kinetic consequences, depending on the reaction, impairing the catalytic efficiency toward phenanthrene 9,10-oxide but enhancing the turnover of CDNB. For example, the turnover number for phenanthrene 9,10-oxide decreases almost 90-fold (from 0.39 to 0.0044 s^{-1}), while that for CDNB increases by a factor of 3.6 (from 20 to 72 s^{-1}) upon mutation of Y115 (*9*).

The crystal structure of the native enzyme suggests that the contribution of Y115 to the physical barrier for product

† Supported by Grants R01 GM30910, P30 ES00267, and T32 ES07028 from the National Institutes of Health.

* To whom correspondence should be addressed. E-mail: r.armstrong@vanderbilt.edu. Fax: (615) 343-2921. Telephone: (615) 343-2920.

‡ Vanderbilt University School of Medicine.

§ University of Maryland and National Institute of Standards and Technology.

[1] Abbreviations: GSH, reduced glutathione; GSO_3^-, glutathione sulfonate; rGSTM1-1, rat glutathione transferase isoenzyme M1-1; CDNB, 1-chloro-2,4-dinitrobenzene; DTNB, dithiobis(2-nitrobenzoic acid); DTT, dithiothreitol; MOPS, 3-(*N*-morpholino)propanesulfonic acid; EDTA, ethylenediaminetetraacetic acid; IPTG, isopropyl thioglucopyranoside; PCR, polymerase chain reaction; GPR, (9*R*,10*R*)-9-(*S*-glutathionyl)-10-hydroxyl-9,10-dihydrophenanthrene; GSDNB, 1-(*S*-glutathionyl)-2,4-dinitrobenzene; PDB, Protein Data Bank.

10.1021/bi026776p CCC: $22.00
Published on Web 11/21/2002

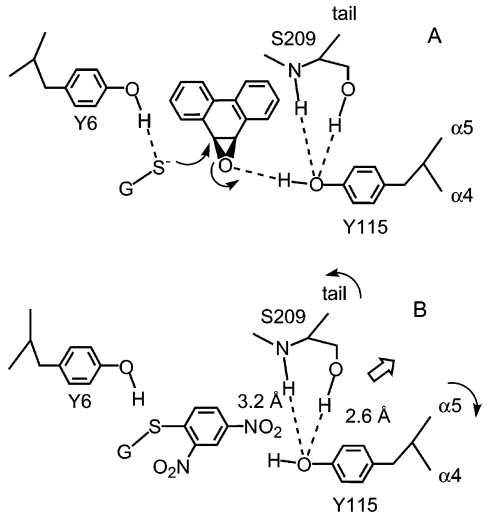

FIGURE 1: (A) Proposed role of Y115 as an electrophilic catalytic group in the addition of GSH to arene oxide substrates. (B) Proposed hydrogen bonding interactions between the hydroxyl group of Y115 and S209 that inhibit segmental motions of the C-terminal tail and the α4 and α5 helices and limit the rate of product release. The large arrow indicates the pathway for egress of product from the active site, while the curved arrows suggest the segmental motions necessary for product release.

release involves hydrogen bonding interactions between the hydroxyl group of Y115, located at the end of the α4 helix, and the side chain hydroxyl group and the main chain amide NH group of S209, located in the C-terminal tail (*8*, *9*). These interactions are proposed to restrain the segmental motion of the two major structural elements (the α4−turn−α5 helices and the C-terminal tail) that form a portion of the 19 Å deep channel to the active site and control the rate of release of product. However, to this point, there has been no direct information regarding the nature of the changes in protein structure or dynamics that might support this proposition.

Conformational changes and protein dynamics are known to be important factors in the catalytic efficiency of enzymes (*10*). In this paper, we demonstrate the utility of backbone amide proton exchange kinetics in detecting segmental motions in the rGSTM1-1 enzyme that directly influence catalysis. We present evidence that the chemical reaction of enzyme-bound GSH and CDNB occurs at a rate 20−50 times faster than product release with both the native enzyme and the Y115F mutant. Crystallographic observations and evidence from amide proton exchange kinetics are consistent with localized increases in the degree of segmental motion of the Y115F mutant that are coupled to enhanced product release. Not surprisingly, the crystal structure of the mutant is very similar to that of the native enzyme. However, the loss of hydrogen bonding interactions involving the hydroxyl group of Y115 is reflected in subtle alterations in the backbone position, an increase in *B*-factors for structural elements that comprise the channel to the active site, and, most dramatically, a loss of well-defined electron density near the site of mutation. The kinetics of amide proton exchange are also enhanced in these regions, providing direct, quantitative evidence for changes in local protein dynamics affecting product release.

EXPERIMENTAL PROCEDURES[2]

Materials. Deuterium oxide (99.9 at. % D), pepsin, neurotensin, angiotensin II, 1-chloro-2,4-dinitrobenzene, glutathione, glutathione sulfonate, and protease inhibitor solution were purchased from Sigma (St. Louis, MO). Trifluoroacetic acid (peptide synthesis grade) was purchased from Pierce Chemicals (Rockford, IL). Acetonitrile (HPLC grade) was purchased from EM Science (Gibbstown, NJ). Anhydrous monobasic potassium phosphate was purchased from Fisher Scientific (Pittsburgh, PA). Benzonase and pET20b(+) were purchased from Novagen (Madison, WI). *PfuTurbo* DNA polymerase was purchased from Stratagene (La Jolla, CA) and Quick T4 DNA Ligase from New England BioLabs Inc. (Beverly, MA). All materials were used without further purification. All the solutions were prepared and used on the same day.

Preparation of the Y115F Mutant. The Y115F mutant used for crystallography was produced as previously described (*9*). A new, more convenient expression vector was prepared for production of the mutant protein for other experiments. The Y115F mutation was introduced into the DNA fragment encoding rGSTM1-1 by a PCR-based method using *PfuTurbo* DNA polymerase. The first PCR was carried out with the 5′-primer AAA AAA TCT AGA CAT ATG CCT ATG ATA CTG GGA TAC TGG (P1) containing the restriction site for *Nde*I, the 3′-primer GCT TCT CAA AGT CGG GGT TGA AAC AAA GCA TGA TGA GC (P2) containing the mutation (underlined), and plasmid pGT33MX encoding rat GSTM1-1 as the template. The second PCR was carried out with the 5′-primer GCT CAT CAT GCT TTG TTT CAA CCC CGA CTT TGA GAA GA (P3) containing the mutation (underlined), the 3′-primer TTT GGA TCC GAA TTC CTA CTT GTT ACT CCA TTG GGC (P4) containing the restriction site for *Eco*RI, and plasmid pGT33MX as the template. Products of both PCRs (DNA fragments of ∼400 bp) were purified by gel electrophoresis and used as templates for the third PCR. This PCR was carried out using primers P1 and P4, and the PCR product (∼600 bp) was purified by gel electrophoresis. The PCR product from the third reaction and the vector pET20b(+) were digested with restriction enzymes *Nde*I and *Eco*RI, purified, ligated with Quick T4 DNA ligase according to the manufacturer's instructions, and transformed into DH5α supercompetent cells. Plasmids obtained from the colonies were purified with the Wizard Plasmid Purification Kit (Promega, Madison, WI) and sequenced to ensure the correct mutation and the absence of secondary mutations.

The mutant plasmid was transformed into BL21(DE3) competent cells. The cells were grown in LB medium containing 150 mg/L ampicillin at 37 °C. Protein expression was induced with 0.3 mM IPTG. Cells were harvested by centrifugation at 6000*g* for 15 min and suspended in 50 mM Tris buffer containing 1 mM EDTA and 1 mM DTT (pH 7.5). The cells were sonicated; 1 mL of 10× protease inhibitor solution was added, and the mixture was centrifuged

[2] Certain commercial materials, instruments, and equipment are identified in this paper to specify the experimental procedure as completely as possible. In no case does such identification imply a recommendation or endorsement by the National Institute of Standards and Technology, nor does it imply that the materials, instruments, or equipment identified is necessarily the best available for the purpose.

at 35000*g* for 35 min. The supernatant was treated with benzonase for 2 h at room temperature to remove nucleic acids and dialyzed against 20 mM MOPS buffer containing 1 mM EDTA and 1 mM DTT (pH 6.8). The protein was loaded on the SP-Sepharose column equilibrated with the same buffer and eluted with an NaCl gradient (from 0 to 500 mM) in the same buffer. Fractions containing protein were pooled together and dialyzed against 20 mM potassium phosphate buffer containing 1 mM EDTA and 1 mM DTT (pH 6.8). The protein solution was loaded onto a hydroxyapatite column and eluted with a buffer gradient (from 20 to 400 mM potassium phosphate) containing 1 mM EDTA and 1 mM DTT (pH 6.8). Fractions containing protein were combined, dialyzed against 20 mM potassium phosphate buffer containing 1 mM EDTA and 1 mM DTT (pH 7.0), concentrated, flash-frozen, and stored at −80 °C.

Measurement of the Rate of the Chemical Reaction. The pre-steady-state measurements of the rate of the chemical reaction in the ternary E·GSH·CDNB complex were taken using an Applied Photophysics SX18MV stopped-flow instrument equipped with two monochromators. All reported concentrations are those in the observation cell after mixing. Reactions were carried out with 10 μM enzyme in 0.1 M potassium phosphate buffer (pH 7.0) containing 1 mM GSH by rapid mixing with different concentrations (50−500 μM) of CDNB prepared in the same buffer. Product formation was followed at 340 nm in a 0.2 cm path length cell maintained at 24 °C. In general, seven-trace averages were accumulated and the kinetic data fit to a theoretical expression describing a single exponential followed by a steady state. The concentration dependence of the observed rate constant for the burst phase followed saturation kinetics from which the rate of the chemical reaction step was derived.

Crystallographic Data Collection. Low-temperature X-ray diffraction data were collected from a single crystal of the mutant enzyme Y115F in complex with (9*R*,10*R*)-9-(*S*-glutathionyl)-10-hydroxy-9,10-dihydrophenanthrene (GPR) using a Bruker electronic area detector and a Rigaku rotating anode X-ray source, as previously described (*8*). The crystals of the Y115F·GPR complex were first transferred to a cryoprotectant solution containing 25% glycerol, 65% ammonium sulfate, and 10 mM Tris buffer, after an initial transfer to a similar solution containing 10% glycerol, before being mounted on a nylon loop and placed on the goniostat. The crystal was maintained at 143 ± 2 K during data collection using a modified Enraf−Nonius cryostat. Data processing was carried out with the XENGEN suite of programs (*11*). The Y115F variant crystallized in space group *C*2. A summary of the data collection and processing statistics is presented in Table 1.

Crystallographic Refinement. The starting model for the refinement of the Y115F structure was the 1.9 Å native structure with the same bound inhibitor, 3GST (*12*), after deletion of the solvent molecules. XtalView (*13*) was used to view the model graphically and to adjust the model during refinement. SHELX (*14*) was used to refine the model against the diffraction data. A summary of the refinement statistics is presented in Table 1. The final coordinates and structure factors have been deposited in the Protein Data Bank (*15*) as PDB entry 1MTC.

Fluorescence Spectroscopy. Steady-state fluorescence spectra were recorded with a Fluorolog-3 spectrofluorometer (Jobin Yvon Horiba Inc., Edison, NJ) equipped with temperature control units. The protein concentration was 3 μM for both the native and mutant enzyme, dialyzed in 20 mM potassium phosphate buffer (pH 7.0). Measurements were recorded at 25 °C using a quartz cell with a path length of 10 mm, and each sample was allowed to reach thermal equilibrium. Fluorescence scans were recorded between 300 and 400 nm using excitation wavelengths between 275 and 295 nm. Also, measurements were taken in the presence or absence of GSH (2 mM) after a 5 min incubation period. All resultant spectra were corrected by subtraction of the background obtained with buffer alone.

Table 1: X-ray Data Collection, Processing, and Refinement Statistics

diffraction data	
space group	*C*2
cell parameters [*a*, *b*, *c* (Å); α (deg)]	85.75, 68.58, 80.46; 105.12
wavelength of data collection (Å)	1.54
highest-resolution shell (Å)	2.26−2.20
R_{merge} (%) (overall/high-resolution shell)	0.11/0.23
completeness (%) (overall/high-resolution shell)	94/91
redundancy (overall/high-resolution shell)	3/3
$\langle I/\sigma I \rangle$ (overall/high-resolution shell)	33/8
refinement	
refinement program	SHELX
resolution limits (Å)	10.0−2.2
unique data (10−2.2 Å)	21775
R_{factor}	0.203
content of the asymmetric unit	intact dimer
no. of residues per monomer	217
no. of inhibitors per monomer	1
no. of water molecules	185
bond length deviation (Å)	0.011
angle distances (Å)	0.039
Ramachandran plot allowed + most favored regions (%)	99.3
average *B* [main chain/side chain (Å^2)]	28.8/30.8

Circular Dichroism Spectroscopy. Steady-state circular dichroism measurements of the native and Y115F mutant enzyme were recorded on a JASCO J-720 spectropolarimeter (Spectroscopic Co. Ltd., Tokyo, Japan) equipped with a data processor. The protein concentration was 30 μM for both near- and far-UV CD measurements, prepared in 20 mM KH_2PO_4 (pH 7.0). Measurements were recorded at 25 °C in the presence or absence of GSO_3^- (3 mM). A quartz cell with a path length of 10 mm was used for near-UV CD (255−350 nm) measurements, while a cell with a path length of 1 mm was used for far-UV CD (180−255 nm) measurements. A total of 15 scans were recorded and averaged for each sample and corrected by subtraction of a baseline with buffer only.

Protein Preparation for H−D Exchange Experiments. Protein samples for H−D exchange experiments were dialyzed against 0.1 M potassium phosphate buffer (pH 6.9) overnight and were filtered prior to use through a 0.2 μm filter to remove particulate matter and any insoluble protein. A stock solution at a concentration of 500 μM (13 mg/mL) was flash-frozen and stored at −80 °C in small aliquots. Each aliquot was sufficient for 20 deuterium exchange mass spectrometric analyses and was used within 1 day of thawing.

Identification of Peptic Fragments. Peptides produced by pepsin digestion of rGSTM1-1 are difficult to predict from sequence alone. Therefore, peptides generated by pepsin digestion of the native protein (1:1 enzyme−substrate

complex) under the quenching conditions used in this study (5 min, pH 2.4, 0 °C) were identified by off-line HPLC and MALDI mass spectrometry. The digest was separated by reverse-phase HPLC, using a 45 min 5 to 45% gradient of acetonitrile on a Beckman Ultrasphere C18 column (4.6 mm × 250 mm), and the elution of the peptides was monitored by absorption at 214 nm. Fractions were collected, dried, and analyzed by MALDI-MS to determine the molecular weights of the peptides. The identities of the peptides were determined by analysis of the computer-generated peptic fragmentation of the native protein using the ExPASy-PeptideMass software (*16*). In cases where mass searching gave more than one possibility, peptides were identified by sequencing with Edman degradation or confirmed by LC−MS/MS sequencing conducted "on the fly" as peptides are eluted out of the column. For MALDI-MS, calibration was performed using a two-point external standard calibration with neurotensin (mass of 1672.92) and angiotensin II (mass of 1046.54). Once optimized, the pepsin digestion was found to be highly reproducible (*17*, *18*).

Hydrogen−Deuterium Exchange. Hydrogen−deuterium exchange experiments were designed to be similar to those reported previously by others (*19*−*22*). Deuterium exchange was initiated by diluting 10 μL of the equilibrated protein solution (13 mg/mL) 10-fold with 90 μL of D_2O. The protein/D_2O solution was incubated at 24 °C for various times (from 10 s to 6 h). At each time point, the reaction was quenched by cooling (tubes transferred to an ice bath) and acidifying with 100 μL of quench buffer [0.1 M potassium phosphate buffer (pH 2.4) in H_2O at 0 °C]. After 30 s, 10 μL of pepsin (12 mg/mL in H_2O at 0 °C) was added to the quenched sample and incubated on ice for 5 min. All the samples for one protein (16 time points) were prepared individually and run on the same day.

Electrospray Ionization Mass Spectrometry. The extent of deuterium incorporation into the peptide fragments was determined by HPLC−MS. The HPLC injection loop and the column were completely submerged in an ice−water slurry at 0 °C to minimize the deuterium back-exchange (*19*). The mixture of peptides was separated in 12 min by a 5 to 60% acetonitrile/H_2O gradient, where both mobile phases contained 0.05% trifluoroacetic acid. The HPLC system consisted of an Alliance 2690 Separations Module (Waters Corp., Milford, MA) equipped with a microbore C18 reverse-phase column, 1 mm × 50 mm (Phenomenex, Torrance, CA). The flow rate through the column was 100 μL/min. A Rheodyne 7125 six-port switching valve (Rheodyne, L.P., Rohnert, CA) was used to divert early-eluting phosphate salts to waste.

Mass determinations were performed using positive ion ESI on a Finnigan MAT TSQ-7000 triple-quadrupole mass spectrometer (Finnigan Corp., San Jose, CA) equipped with a standard API-1 electrospray ionization source outfitted with a 100 μm inside diameter deactivated fused silica capillary. The heated capillary was operated at 150 °C and 40 V, and the tube lens voltage was set to 120 V to minimize formation of H_2O−solvent clusters. The mass spectrometer was operated in the positive ion mode, and the spray voltage was maintained at 4 kV. Nitrogen was used for both the sheath and auxiliary gas. The detector was calibrated to unit resolution, and the data were collected by scanning from *m*/*z* 300 to 900 with a scan time of 2 s.

Data acquisition and spectral analysis were conducted with Finnigan ICIS software, version 8.3.2., on a Digital Equipment Corp. Alpha workstation. Additional data processing was performed using Finnigan Xcalibur software, version 1.2. The centroid data were analyzed using MagTran 1.0 beta 9 software written by Zhang and Marshall (*23*). Peptide ions were located by scanning, and intensities of all scans containing the peptide were summed to produce a composite spectrum for each ion. Data were processed by calculating the centroid of the resulting ion spectra.

Kinetic Analysis. The amount of deuterium in each peptide was adjusted for back-exchange (as described below) and plotted versus time. Progress curves for individual peptides were fitted using the program Grafit (Erithacus Software) to the sum of first-order rate terms according to the equation

$$D = N - \sum_{i=1}^{N} \exp(-k_i t)$$

where D is the deuterium content of a peptide, N is the number of peptide amide protons, k_i is the exchange rate constant for each amide hydrogen, and t is the time allowed for isotopic exchange.

Deuterium Exchange Control Experiments. A zero time control ($m_{0\%}$) was performed to determine the extent of in-exchange that occurred after acidification and during the pepsin digestion, even though the isotopic exchange rate is quenched at this temperature and pH (*24*). The sample was prepared by adding 10 μL of protein to 100 μL of quench buffer at 0 °C, followed by the addition of 90 μL of D_2O, digestion, and analysis by the normal procedure. The amount of deuterium gained during the analysis varied between 0 and 10%.

To determine the amount of deuterium lost during the HPLC fractionation, a completely deuterated protein sample ($m_{100\%}$) was prepared by incubating the protein in D_2O at 50 °C for 3 h at neutral pH, followed by incubation at pH 2.5 and 50 °C for an additional 3 h (*19*, *24*). The sample was then incubated on ice for a few minutes, digested, and analyzed by the normal procedure. The average amount of deuterium lost during analysis was 16% after normalizing to 100% deuterium.

The deuterium contents of partially deuterated peptides, adjusted for the gain and loss of deuterium during analysis, were obtained from the following expression (*24*):

$$D = \left[\left(\frac{m_t - m_{0\%}}{m_{100\%} - m_{0\%}}\right)N\right]/0.9$$

where D is the deuterium content in a particular peptide and $m_{0\%}$, m_t, and $m_{100\%}$ are the average molecular weights of the same peptide in the zero-time control, partially deuterated sample, and fully deuterated control, respectively. The total number of peptide amide protons is given by N with division by 0.9 to normalize to 100% D_2O.

RESULTS

Kinetics of Chemical Catalysis by the Native Enzyme and Y115F Mutant. To further substantiate the contention that product release is the rate-limiting step in the rGSTM1-1-catalyzed reaction of GSH and CDNB, the pre-steady-state

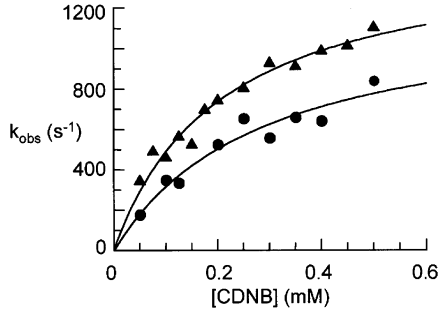

FIGURE 2: Dependence of the observed rate constant for the burst of product on CDNB concentration. The data for the native enzyme (●) and Y115F mutant (▲) were fit to eq 2 by nonlinear regression with the following values: $k_{chem} = 1200 \pm 200\ s^{-1}$ and $K_d^{CDNB} = 280 \pm 90\ \mu M$ for the native enzyme and $k_{chem} = 1500 \pm 100\ s^{-1}$ and $K_d^{CDNB} = 210 \pm 30\ \mu$ for the mutant.

kinetics of the reaction were examined. As expected, burst kinetics were observed with both the native enzyme and the Y115F mutant. The reactions were followed to no more than 10% substrate consumption, and the data were fit to a burst followed by a steady state. The observed rate constants for the burst followed saturation kinetics consistent with the mechanism and rate expression shown in eqs 1 and 2 from which k_{chem} and K_d^{CDNB} could be obtained.

$$E{\cdot}GS^- + CDNB \overset{K_d^{CDNB}}{\rightleftharpoons} E{\cdot}GS^-{\cdot}CDNB \xrightarrow{k_{chem}} E{\cdot}GSDNB \xrightarrow{slow} \quad (1)$$

$$k_{obs} = \frac{k_{chem}[CDNB]}{K_d^{CDNB} + [CDNB]} \quad (2)$$

The kinetic results are shown in Figure 2. There is very little difference in k_{chem} or K_d^{CDNB} for the native and mutant enzyme. Most importantly, k_{chem} exceeds k_{cat} by a factor of 60 with the native enzyme and a factor of 20 with the mutant. Clearly, in both cases, the rate-limiting step in turnover is product release.

Crystal Structure of the Y115F Mutant. The overall structure of the Y115F mutant is essentially the same as that of the native enzyme as illustrated in Figure 3. The rms deviation of the Cα positions from those of the native enzyme (PDB entry 3GST) is 0.35 Å for all 434 residues. However, there are significant local changes in the structure manifested in both the quality of the electron density and conformation. Although the F115 residue has well-defined electron density in chain A (Figure 4A), no electron density for this residue is evident in the σ_A-weighted $2F_o - F_c$ electron density map of the B chain as illustrated in Figure 4B. The displacement of the Cα atoms for the F115 residues is larger than average (0.5 and 0.6 Å for subunits A and B, respectively) as the residues move closer to the phenanthrene ring of the product inhibitor.

In the native structure, the hydroxyl group of Y115 is within hydrogen bonding distance of both the hydroxyl group and the amide NH group of S209 (Figures 1 and 3). Thus, the removal of the hydroxyl group from residue 115 eliminates these potential hydrogen bonding interactions and transmits the conformational perturbations to residues in the C-terminal tail, including S209 in the mutant structure. The side chain of K210, immediately following S209, forms an ionic interaction with the carboxylate of D36 in the mu loop of the native enzyme. This interaction is also disrupted in the mutant. The B chain of the dimer displays considerably more disruption than does the A chain as is evident from the poorer electron density of the B chain in this region and in the greater increase of the *B*-factors from the normalized value for the whole structure. A marked difference in the *B*-factors of the A and B chains was also noted and discussed in some detail in the original report of the native structure (*8*).

The different crystallographic behavior of the A and B chains appears to arise from lattice interactions which stabilize the conformation of the A chain in the region near the mutation. The crystal packing in the region of F115 in the A chain is shown in Figure 5. In a similar view of the B chain (not shown), no neighboring molecule is visible. Crystallographic data were also collected at room temperature (unpublished results). In the room-temperature structure, the dynamic disorder of the mutant is increased to the extent that there is no visible electron density for B chain residues 114−126 and 208−217.

Spectral Properties of the Y115F Mutant. The changes in the fluorescence and CD spectra of the Y115F mutant are modest and consistent with the loss of a single tyrosine chromophore (Figures S1−S4 of the Supporting Information). The near-UV CD spectrum of the mutant shows a small decrease in ellipticity near 280 nm. The fluorescence emission spectrum of the mutant, centered at 335 nm, is slightly more intense than that of the native enzyme, suggesting that Y115 is responsible for some quenching of the intrinsic tryptophan emission in the native enzyme. There is no spectral evidence for a large disruption of structure in the mutant protein.

Kinetics of Amide Proton Exchange. The kinetics of amide proton exchange were monitored by ESI-TOF mass spectroscopy over a time window of 10 s to 6 h for each of 50 peptides identified in the peptic peptide map of the native and mutant proteins. The 50 peptides, ranging in size from 3 to 18 residues, cover 100% of the 217-residue sequence with 64% of the sequence represented by multiple peptides (Figure S5 of the Supporting Information). In most instances, the amide exchange kinetics can be resolved into three phases, including a burst of rapidly exchanging protons ($k_x > 4\ min^{-1}$), an intermediate phase ($4\ min^{-1} > k_x > 0.04\ min^{-1}$), and a very slow phase ($k_x < 0.04\ min^{-1}$). The reproducibility of the kinetic profiles for all 50 peptides was confirmed by a second, independent determination of the exchange kinetics.

Not surprisingly, the amide exchange kinetics for most (>70%) of the main chain remain unaffected by the single mutation. No regions show an increase in the magnitude of the burst phase. However, several regions of the protein show enhanced amide proton exchange in the intermediate phase. The most prominent of these regions includes the end of the α4 helix−turn−α5 helix junction that harbors the mutation (residues 111−120), residues 209−217 in the C-terminal tail, and the mu loop (residues 34−46). The kinetic data for the amide proton exchange in these regions are illustrated in Figures 6−9, respectively. Kinetic profiles for H−D exchange in representative peptides covering the remainder of the protein sequence are shown in Figures S6−S10 of the Supporting Information.

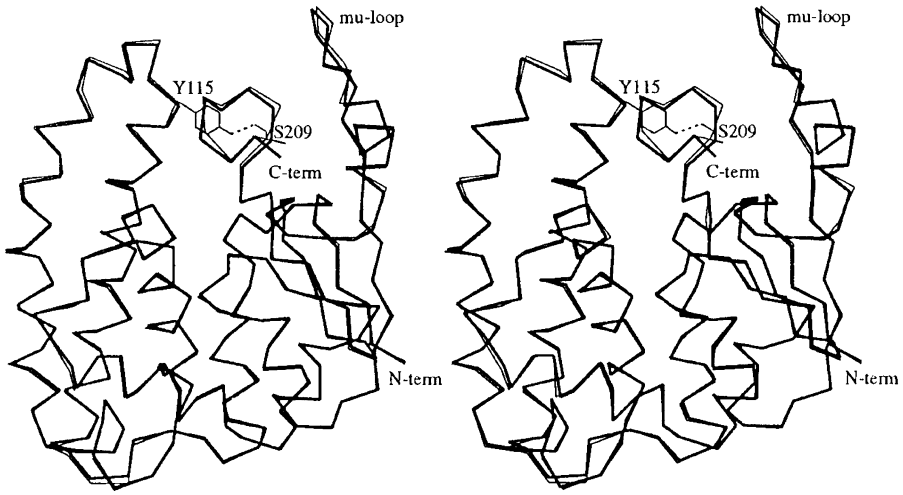

FIGURE 3: Stereoview of the superposition of the α-carbon trace of subunit B of the native enzyme (thin line) and the Y115F mutant (thick line). The side chains of Y115 and S209 involved in the hydrogen bonding interactions are illustrated for the native enzyme.

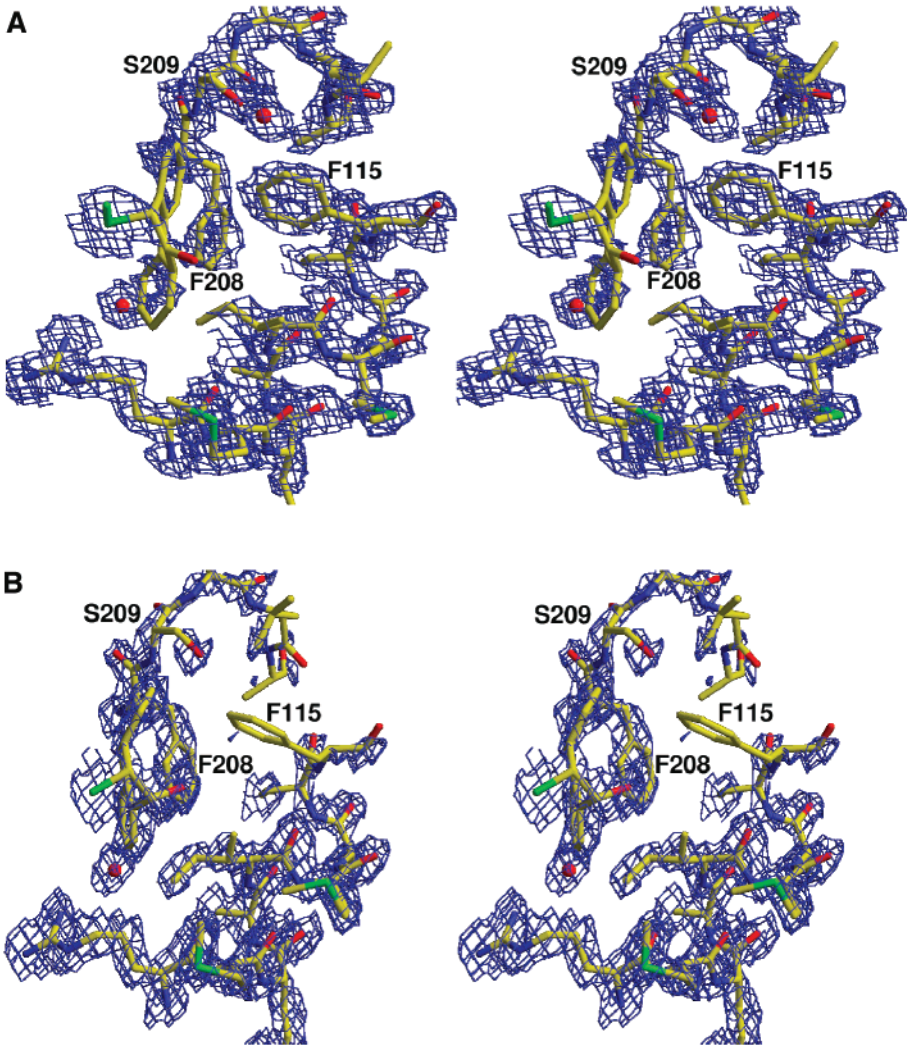

FIGURE 4: Stereoview of the $2F_o - F_c$ electron density maps contoured at 1σ in the region near F115 in the Y115F mutant. The regions in subunits A and B are shown in panels A and B, respectively.

Amide Proton Exchange Near the Site of Mutation. Peptic peptide 114−126 containing the site of mutation shows a burst of four deuterons incorporated in the fast phase followed by approximately five in the intermediate phase and one in the slow phase as illustrated in Figure 6. The kinetic behavior of the native enzyme and that of the Y115F mutant are the same except for the rate constant in the intermediate exchange regime which approximately doubles in the mutant. The kinetic situation near the site of mutation can be further clarified by subtracting the observed time course of exchange for the overlapping peptic peptide 120−126 that includes the α5a helix from peptide 114−126.

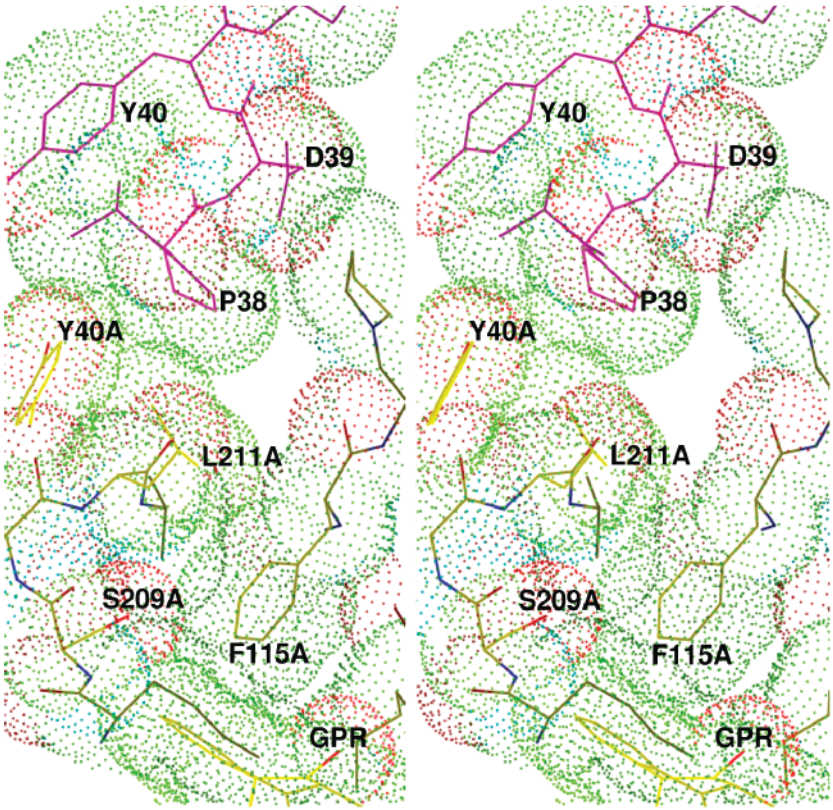

FIGURE 5: Crystal contacts in the region of F115 of chain A of the Y115F mutant. The skeleton of a crystallographic neighbor is shown in hot pink. The dots represent the van der Waals surface of the protein.

Peptide 120−126 (Figure 6B) shows a burst of one to two deuterons followed by intermediate and slow phases involving two deuterons and one deuteron, respectively. The kinetic behavior of the native and mutant enzymes is similar in all three phases.

Thus, the difference between the two peptides gives a much clearer picture of the effect of the mutation on the exchange behavior for the amide protons between residues 114 and 120 as illustrated in Figure 6C. This region shows a burst of 2.5−3 deuterons and an intermediate exchange of two deuterons with the primary kinetic difference being an ~3-fold increase in the rate constant for exchange in the intermediate phase of the mutant.

The C-terminal end of the α4 helix, peptide 111−113, which precedes the site of mutation, exhibits enhanced amide exchange as shown in Figure 7. This region shows essentially no burst phase and a rather slow overall exchange with one amide proton exchanging in the intermediate phase and one in the slow phase. The exchange behavior is consistent with the fact that this helix resides in the center of the molecule with little exposure to solvent. Although there is considerable similarity between the exchange reaction in the native and mutant proteins, the rate constant observed for the proton in the intermediate phase in the mutant is 6.8 times larger than that for the native enzyme.

Amide Proton Exchange Distal to the Site of Mutation. The changes in amide proton exchange kinetics are not confined to the immediate sequence around the mutation. The C-terminal tail, peptide 209−217, also exhibits enhanced amide proton exchange in the intermediate phase as illustrated in Figure 8A. This relatively solvent exposed peptide shows a burst of seven deuterons incorporated followed by a single deuteron in the intermediate phase. Again, the only significant difference observed in the kinetics of the native and mutant proteins is a 10-fold increase in the rate constant for intermediate exchange in the mutant. As before, the exchange data for an overlapping peptide 212−217 (Figure 8B) can be used to help isolate the amide exchange site that is altered by the mutation. Thus, subtraction of the exchange data for peptide 212−217 from that for the larger peptide (209−217) suggests that the amide site that gives rise to intermediate exchange is located between residues 209 and 212 (Figure 8C). The SKLA tetrapeptide for the mutant protein has a burst of three deuterons and again exhibits a 10-fold increase in the rate constant for the intermediate phase exchange of a single proton. In principle, the rate constants for the intermediate phase in peptide 209−217 (Figure 8A) and residues 209−212 obtained via the difference should be the same. The fact that they are not derives from the noise level in the kinetic data of approximately ±0.2 deuteron.

The C-terminal tail is also in contact with the mu loop in domain I (residues 35−41) via an ionic interaction between the side chains of K210 and D36. This interaction appears to be disrupted in the crystal structure of Y115F. The structural perturbation can also be detected in the amide exchange kinetics of the mu loop. The amide exchange in this region, embodied in peptic peptide 34−46, which includes the mu loop and the α2 helix, is illustrated in Figure 9. The exchange behavior of each peptide consists of a burst of seven deuterons, and intermediate and slow kinetic phases of two deuterons each. The principal difference is a 2.8-fold increase in the rate constant for the intermediate phase of the exchange.

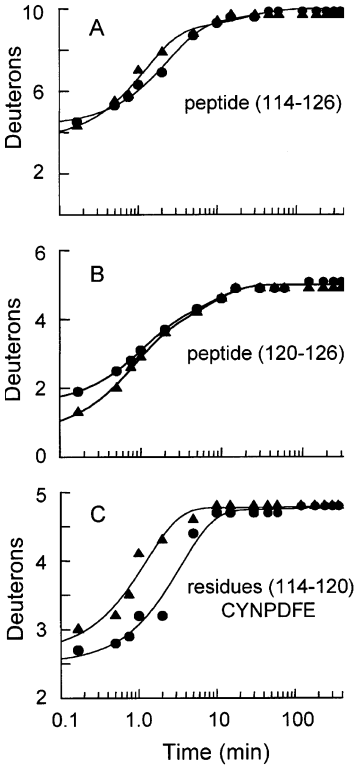

FIGURE 6: Kinetics of amide proton exchange for the native and Y115F proteins near the site of mutation. (A) For peptide 114−126, the experimental data for the native enzyme (●) and Y115F mutant (▲) were fit to a double exponential with the following values: $A_1 = 4.8 \pm 0.3$ D, $k_{ex1} = 0.42 \pm 0.05$ min^{-1}, $A_2 = 0.9 \pm 0.3$ D, and $k_{ex2} = 0.04 \pm 0.02$ min^{-1} for the native enzyme and $A_1 = 5.3 \pm 0.5$ D, $k_{ex1} = 0.8 \pm 0.2$ min^{-1}, $A_2 = 1.1 \pm 0.4$ D, and $k_{ex2} = 0.04 \pm 0.03$ min^{-1} for the mutant. (B) For peptide 120−126, the experimental data for the native enzyme (●) and Y115F mutant (▲) were fit to a double exponential with the following values: $A_1 = 2.1 \pm 0.3$ D, $k_{ex1} = 1.1 \pm 0.2$ min^{-1}, $A_2 = 1.4 \pm 0.3$ D, and $k_{ex2} = 0.13 \pm 0.03$ min^{-1} for the native enzyme and $A_1 = 2.7 \pm 0.3$ D, $k_{ex1} = 1.3 \pm 0.3$ min^{-1}, $A_2 = 1.6 \pm 0.3$ D, and $k_{ex2} = 0.15 \pm 0.03$ min^{-1} for the mutant. (C) Amide exchange of residues 114−120 by subtraction of peptide 120−126 from peptide 114−126. The difference data for the native enzyme (●) and Y115F mutant (▲) were fit to a single exponential with the following values: $A = 2.27 \pm 0.08$ D and $k_{ex} = 0.27 \pm 0.03$ min^{-1} for the native enzyme and $A_1 = 2.1 \pm 0.1$ D and $k_{ex1} = 0.77 \pm 0.09$ min^{-1} for the mutant.

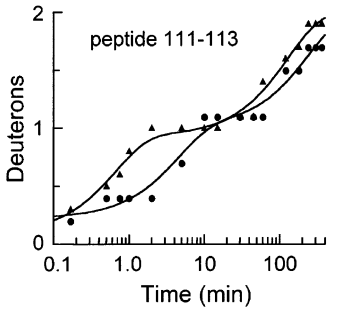

FIGURE 7: Kinetics of amide proton exchange in the native and Y115F proteins in the C-terminal half of the α4 helix (residues 111−113). The experimental data for the native enzyme (●) and Y115F mutant (▲) were fit to a double exponential with the following values: $A_1 = 0.78 \pm 0.08$ D, $k_{ex1} = 0.22 \pm 0.07$ min^{-1}, $A_2 = 0.99 \pm 0.07$ D, and $k_{ex2} = 0.0040 \pm 0.0006$ min^{-1} for the native enzyme and $A_1 = 0.8 \pm 0.1$ D, $k_{ex1} = 1.5 \pm 0.4$ min^{-1}, $A_2 = 1.07 \pm 0.04$ D, and $k_{ex2} = 0.0076 \pm 0.0008$ min^{-1} for the mutant.

One other region (residues 46−62) of the Y115F mutant has altered amide proton exchange behavior that is manifest primarily in the burst phase. The five peptic peptides that cover this region (peptides 49−62, 49−59, 49−56, 46−56, and 51−62) all show a decrease in the amplitude of the burst phase of Y115F by one deuteron with a concomitant increase

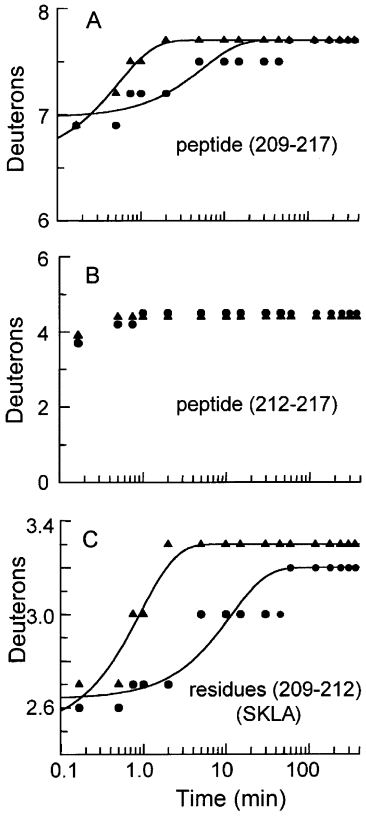

FIGURE 8: Kinetics of amide proton exchange for the native and Y115F proteins in the C-terminal tail. (A) For the peptide 209−217, the experimental data for the native enzyme (●) and Y115F mutant (▲) were fit to a single exponential with the following values: $A = 0.72 \pm 0.07$ D and $k_{ex} = 0.18 \pm 0.06$ min^{-1} for the native enzyme and $A = 1.11 \pm 0.05$ D and $k_{ex} = 1.9 \pm 0.1$ min^{-1} for the mutant. (B) For peptide 212−217, the experimental data for the native enzyme (●) and Y115F mutant (▲) were not fit to a kinetic expression since the change in the deuterium level is defined by a single time point. (C) Amide exchange of residues 209−212 by subtraction of peptide 212−217 from peptide 209−217. The difference data for the native enzyme (●) and Y115F mutant (▲) were fit to a single exponential with the following values: $A = 0.56 \pm 0.04$ D and $k_{ex} = 0.09 \pm 0.03$ min^{-1} for the native enzyme and $A = 0.79 \pm 0.0.07$ D and $k_{ex} = 1.1 \pm 0.2$ min^{-1} for the mutant.

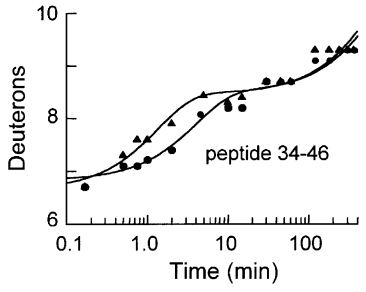

FIGURE 9: Kinetics of amide proton exchange for the native and Y115F proteins in the mu loop, peptide 34−46. The experimental data for the native enzyme (●) and Y115F mutant (▲) were fit to a double-exponential expression with the following values: $A_1 = 1.7 \pm 0.1$ D, $k_{ex1} = 0.25 \pm 0.07$ min^{-1}, $A_2 = 2.5 \pm 0.1$ D, and $k_{ex2} = 0.0014 \pm 0.0003$ min^{-1} for the native enzyme and $A_1 = 1.8 \pm 0.2$ D, $k_{ex1} = 0.7 \pm 0.2$ min^{-1}, $A_2 = 2.5 \pm 0.1$ D, and $k_{ex2} = 0.0016 \pm 0.0003$ min^{-1} for the mutant.

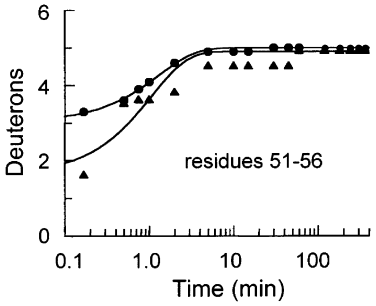

FIGURE 10: Kinetics of amide proton exchange for residues 51−56 in the native and Y115F mutant enzymes. The segment was analyzed with the double-difference procedure described in the text. The difference data for the native enzyme (●) and Y115F mutant (▲) were fit to a single exponential with the following values: $A = 1.96 \pm 0.05$ D and $k_{ex} = 0.76 \pm 0.04$ min^{-1} for the native enzyme and $A = 3.3 \pm 0.3$ D and $k_{ex} = 0.9 \pm 0.2$ min^{-1} for the mutant.

in the amplitude of the intermediate phase (see Figure S7 of the Supporting Information). A double-subtraction procedure was used to further localize the altered exchange kinetics. In this instance, the difference in the time course for exchange of [49−62] − [49−56] was calculated. The resulting difference, [56−62], was then used to calculate the difference of [51−62] − [56−62] = [51−56]. Kinetic analysis of residues 51−56 in Figure 10 shows that this segment has the same kinetic attributes as all five peptides in this region with a shift of a single deuteron from the burst phase into the slower intermediate exchange regime.

DISCUSSION

Kinetics of Amide Proton Exchange and Protein Structure. The influence of protein structure on the kinetics of amide proton exchange has been discussed extensively by others (*25*−*28*). The GSH transferase investigated herein reveals no real surprises in this regard and therefore will not be discussed in great detail.[3] However, it is instructive to consider the relationship between the structure and changes in the protein dynamics for those regions of the protein affected by the Y115F mutation. The helical regions, for example the α4 and α5 helices that dominate the structure between residues 111 and 126, tend to have relatively few rapidly exchanging amides with most exchanging in the intermediate or slow kinetic regimes. The ends of the α4 and α5 helices and the β-turn (residues 116−119) that connects them show a mixture of exchange kinetics consistent with the structure. In the native structure, all but two of the main chain NH groups in the segment of residues 114−120 harboring the mutation are within hydrogen bonding distance of a main chain C═O group. The two exceptions are the NH group of D118, which is within hydrogen bonding distance of the side chain C═O group of N116, and the NH group of E120, which is exposed to solvent. The latter two NH protons are likely to constitute two of the three that exchange in the burst phase. The principal difference in the hydrogen bonding pattern in the Y115F mutant is the loss of the hydrogen bond between the main chain NH group of N116 and the C═O group of L113. This latter hydrogen bond is in the transition region between the α4 helix and the β-turn and may be the third rapidly exchanging proton. The remaining two NH groups [Y(F)115 in the helix and F119 in the β-turn] are probably the two groups that exchange at intermediate rates and have enhanced rates in the mutant.

In contrast, the loops and meanders that are more exposed to solvent exhibit a completely different kinetic distribution with most amide protons exchanging in the burst phase. Peptide 34−46, which embodies the mu loop and the short α2 helix, contains 11 amide protons, seven of which exchange in the burst phase. The crystal structures reveal four amide NH groups that are engaged in hydrogen bonding interactions, including G35 and Y40 in the loop and W45 and L46 in the helix. These interactions remain unchanged in the structure of the mutant. Similarly, the segment of residues 209−217 in the C-terminal tail is largely solvent exposed and exchanges seven of eight amide protons in the burst phase. The one proton that exchanges in the intermediate phase is probably from A212 which is hydrogen bonded to the C═O group of S209 in the native structure. That interaction appears to be changed in the Y115F mutant, though the structure of the B subunit in this region is not well defined as reflected in the high *B*-factors.

The one region that shows a decrease in amide proton exchange rates, residues 51−56, is involved in subunit−subunit interactions at the dimer interface. The side chain of F56 from one subunit intercalates between the α4 and α5 helices of the opposite subunit (*8*). The observed decrease in the H−D exchange rate might be due to changes in the subunit interface involving the α4 helix and F56. However, there is no discernible difference between the structures of the native and mutant proteins in this region in either subunit that would explain the shift of one amide proton from the burst to the intermediate phase. Although one of the amide protons in this region, that of K51, is involved in a hydrogen bond with the carbonyl oxygen of E48, the others are within hydrogen bonding distance of various water molecules. Given the structural results, it is surprising that more than one proton is found in the intermediate exchange regime. Slow exchange of surface-exposed amides has been observed previously (*22*) and may be a reflection of the fact that conformations other than the one revealed in the crystal structure may predominate in solution.

Structural and Functional Basis for the Role of Y115 in Catalysis. The exact role of active site residues in catalysis can often be deduced from a straightforward combination of crystallographic and functional analysis of mutant enzymes. Our original report of the participation of the hydroxyl group of Y115 in oxirane ring opening reactions was based on just such an analysis (*9*). The proximity of this side chain to the hydroxyl group of the ring-opened product and the dramatic loss of catalytic efficiency of the Y115F mutant toward epoxide substrates provide compelling support for its participation in electrophilic catalysis.

In contrast, the exact structural basis of the influence of Y115 in the enzyme-catalyzed addition of GSH to CDNB is not as well characterized. That the rate-limiting step in turnover of this substrate is the product release step is now firmly established (*9*). In previous work, the reciprocal of the relative turnover number of the reaction was found to exhibit a dependence on viscosity with a unit slope. In addition, direct measurement of k_{off} for the product GSDNB

[3] A more detailed discussion of the relationship of structure to observed amide proton exchange rates is being prepared for a future publication (S. G. Codreanu, D. L. Hachey, H. W. Dirr, and R. N. Armstrong, unpublished results).

Table 2: Segmental Amide Proton Exchange Rate Enhancement and Normalized Changes in *B*-Factors for the Y115F Mutant

peptide or segment	$k_{cat}^{Y115F}/k_{cat}^{N}$	$k_{chem}^{Y115F}/k_{chem}^{N}$	k_x^{Y115F}/k_x^{N} [a]	normalized change in the *B*-factor[b] A	normalized change in the *B*-factor[b] B
intact enzyme	3.6	1.3	−	0.95 (0.99)	1.05 (1.01)
residues 114−120 (α4−turn−α5)			2.9 (2)	1.26 (1.36)	1.95 (1.69)
residues 111−113 (α4)			6.8 (1)	1.32 (1.19)	1.50 (1.45)
residues 209−212 (C-terminal tail)			12 (1)	1.44 (1.27)	2.38 (1.61)
residues 34−46 (mu loop, α2)			2.8 (2)	1.22 (1.38)	1.44 (1.46)

[a] The values in parentheses are the number of amide protons that show enhanced exchange kinetics. [b] Average *B*-factors for individual subunits were normalized by dividing the average for the subunit by the average of the dimer. Average *B*-factors for segments were normalized using the average for the subunit in which the segment resides. Values in parentheses are for the native enzyme.

indicated that $k_{off} \approx k_{cat}$. Furthermore, product release remains the rate-limiting step in the turnover of CDNB by the Y115F mutant (*9*). The direct measurement of the rate of the chemical reaction in the ternary complex reported herein firmly establishes that the chemical step is much faster than turnover in both the native and mutant enzymes. Thus, the increase in turnover number from 20 to 72 s^{-1} in the Y115F mutant must reflect an increase in the off-rate of the product.

Crystallographic analysis of the Y115F mutant suggests that the structural basis for enhanced product release is the loss of the hydrogen bonding interactions between the hydroxyl group of Y115 and S209 in the C-terminal tail of the protein. The poor electron density (and high *B*-factors) for F115 and neighboring residues and residues in the C-terminal tail are consistent with a dynamic or static disorder in the immediate vicinity of the mutation, particularly in the B subunit. The loss of this hydrogen bonding interaction also results in the disruption of the ion pair interaction between K210 and D36 in the mu loop that is evident in the high *B*-factors in this region as well. The disorder in these three parts of the molecule is much less apparent in subunit A due to lattice contacts that stabilize the same region. Thus, the crystallographic characteristics of subunit B probably more accurately reflect the influence of the mutation on the solution structure of the protein. The crystallographic data are consistent with an increase in the degree of segmental motion in these regions of the mutant, but they do not distinguish between static or dynamic disorder.

Amide Proton Exchange Kinetics and Protein Dynamics. The kinetics of amide proton exchange in folded proteins is known to be influenced by both protein structure and dynamics (*27*−*31*). Amide groups exposed to solvent at neutral pH and not involved in intramolecular hydrogen bonding interactions exchange rapidly with intrinsic rate constants (k_i) of ~10 s^{-1} depending on the sequence context. Buried amide groups, which are often involved in hydrogen bonding interactions in secondary structural elements, typically, exchange at much lower rates that depend, in large part, on dynamic fluctuations in the protein structure. The kinetic situation is often expressed in the mechanisms shown in Scheme 1 where $(NH)_c$ is an amide in a closed conformation, (NH_o represents the open conformation, k_o is the rate constant for opening, k_c is the rate constant for closing, and k_i is the intrinsic rate constant for amide proton exchange (*29*). The experimental rate constant for exchange is given by the equation $k_x = k_o k_i/(k_o + k_c + k_i)$. For a folded protein or substructure, $k_c \gg k_o$ so that the rate expression for exchange simplifies to $k_x = k_o k_i/(k_c + k_i)$. If it is also true that $k_c \gg k_i$, then $k_x = k_i k_o/k_c$. Thus, the experimental exchange rate can be expressed in terms of the product of the rate constant for intrinsic exchange and the dynamic factor k_o/k_c, which is the equilibrium constant between the closed and open states. The possibility of exchange directly from the closed state is often accounted for by a probability factor β such that $k_x = (\beta + k_o/k_c)k_I$ (*27*). In either case, the molecular dynamics of the exchange process are embodied in the term k_o/k_c.

Scheme 1

$$(NH)_c \underset{k_c}{\overset{k_o}{\rightleftharpoons}} (NH_o \xrightarrow[D_2O]{k_i} (ND_o \underset{k_c}{\overset{k_o}{\rightleftharpoons}} (ND)_c$$

The increases in the rates of amide proton exchange observed in the Y115F mutant are modest and are transmitted by intramolecular contacts to structural elements distal to the site of mutation. The single mutation is unlikely to affect the intrinsic rate constant for exchange, k_I, or β, particularly for regions away from the mutation. It is therefore likely that the increase in rate is due to an increase in the equilibrium constant for formation of an open conformation (k_o/k_c) from which exchange occurs. It is quite striking that the increases in k_x expressed as the ratio k_x^{Y115F}/k_x^{N} (Table 2) for all of these regions fall in a very narrow range. For three of these segments, $k_x^{Y115F}/k_x^{N} \approx 3-12$. Moreover, the segments in question are in physical contact with one another as illustrated in Figure 11. The narrow range of enhancement and the physical contact of the segments suggest that the change in molecular dynamics is due to coupled motions in the access channel.

There is a reasonable correlation between the increase in amide proton exchange rates and increases in *B*-factors observed in the crystal structure particularly as seen in the quality of the electron density displayed in Figure 4. However, the correlation is not perfect when normalized *B*-factors between the native and Y115F structures are compared (Table 2). This is due, in part, to crystal lattice effects that dampen segmental dynamics in the A subunit. Three of the four regions compared in subunit B show an increase in normalized *B*-factors in response to the mutation. The fact that the native and mutant structures were determined under different conditions and refined with different protocols may also make comparison of even normalized *B*-factors problematic. Overall, H−D exchange rates appear to be a more sensitive and reliable indicator of changes in protein dynamics since they are free of lattice effects.

Segmental Protein Dynamics and Catalysis. The structural elements most affected by the mutation lie atop the access channel to the active site as illustrated in Figure 11. The influence of protein dynamics on product release where

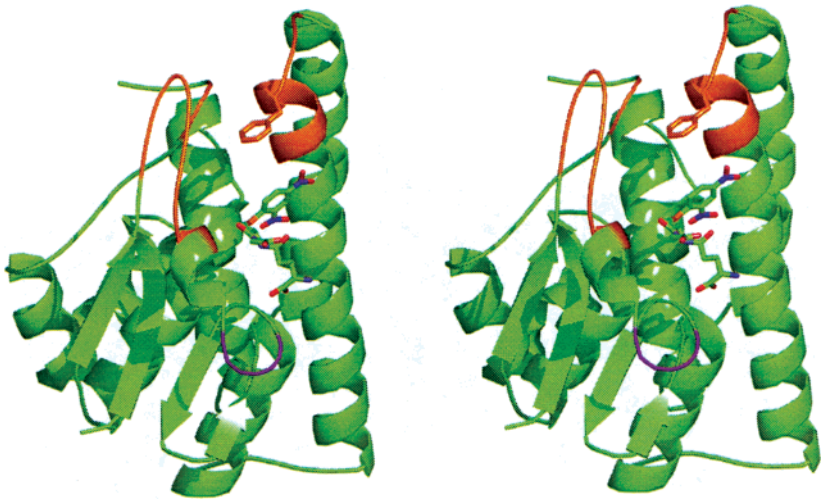

FIGURE 11: Stereoview of the product bound in the active site of the Y115F mutant of rGSTM1-1. The ribbon diagram of a single subunit as viewed from the opposing subunit in the dimer is shown. The product, GSDNB, which is shown in stick representation, was placed in the structure by superposition of the structure of the native enzyme in complex with GSDNB from PDB entry 5GST with the Y115F mutant. Protein segments that lie atop the active site access channel and exhibit enhanced H−D exchange are shown in orange. The single segment that shows a reduced level of amide proton exchange is illustrated in purple. This figure was produced with the program PyMol (*33*).

product release is rate-limiting can be treated kinetically in a manner similar to that described for amide proton exchange. That is, release occurs from an open conformation so that $k_{cat} = k_{off} = (\beta_p + k_{op}/k_{cp})k_{chem}$, where k_{op} and k_{cp} are the rate constants for the transition between the open and closed conformations, respectively, β_p is the probability of release from the closed conformation, and k_{chem} is the rate constant for the chemical step in the ternary complex.[4] Thus,

$$k_{cat}^{Y115F}/k_{cat}^{N} = (\beta_p + k_{op}/k_{cp})^{Y115Y}(k_{chem}^{Y115F})/(\beta_p + k_{op}/k_{cp})^{N}(k_{chem}^{N})$$

This equation can be rearranged to provide the ratio of the dynamic terms so that

$$(k_{cat}^{Y115F}/k_{cat}^{N})(k_{chem}^{N}/k_{chem}^{Y115F}) = (\beta_p + k_{op}/k_{cp})^{Y115Y}/(\beta_p + k_{op}/k_{cp})^{N} = 2.9$$

This value is quite similar to the rate enhancements (k_x^{Y115F}/k_x^{N}) observed in amide proton exchange and suggests that product release and amide exchange are dependent on the same segmental motions.

The term $\beta + k_o/k_c$ expresses the probability of H−D exchange in a folded structure and can be estimated from the k_x/k_i ratio. If $k_i \approx 10$ s^{-1} for an exposed amide proton, then exchange in the intermediate time regime ($k_x = 0.01-0.001$ s^{-1}) reflects an equilibrium constant (k_o/k_c) between the open and closed conformations of perhaps ≤ 0.0001 depending on the magnitude of β. It is difficult to make a similar estimate of k_{op}/k_{cp} since an intrinsic k_{off} from the open conformation is not known nor is β_p. However, the fact that the ratio of the dynamic terms $(\beta_p + k_{op}/k_{cp})^{Y115Y}/(\beta_p + k_{op}/k_{cp})^{N} \approx k_x^{Y115F}/k_x^{N}$ suggests that the relative changes in the equilibrium population of conformers responsible for the two physical processes are similar.

[4] The rate constant k_{chem} is not an intrinsic rate constant for product release but is the limit that cannot be exceeded if product release is the rate-limiting step in turnover.

It is important to point out that product dissociation occurs on the millisecond time scale ($k_{off} = 20-70$ s^{-1}, $t_{1/2} = 10-35$ ms), a time scale that is similar to that expected for the upper limit of large-amplitude segmental motions. The rate constants for the segmental fluctuations in the protein structures are not known in this specific case, but it is likely that they occur on the microsecond to millisecond time scale (*29*, *32*). In fact, Rule and co-workers have suggested, based on residual dipolar couplings, that the motions of the mu loop in a homologous human enzyme (hGSTM2-2) occur on the microsecond to nanosecond time scale with large excursions from the position observed in the crystal structure (*34*). In contrast, the motions of the α4 helix and the C-terminal tail were proposed to occur on a time scale much longer than microseconds. The mutation-induced changes in segmental motions in rGSTM1-1 described herein suggest that the segmental motions of all three structural elements are coupled even if the time scales for their dynamics are different. The success of the H−D exchange experiments reported here relies on the kinetic sampling of changes in the equilibrium position of relatively rapid segmental fluctuations. Extension of the H−D exchange experiment into the millisecond time regime is possible with rapid quench-flow techniques and should permit a much more detailed mapping of changes in protein dynamics and their influence on catalysis.

Conclusions. The results in this report demonstrate that amide H−D exchange mass spectrometry is a sensitive technique for locating and quantifying changes in segmental motions of proteins that are important in diffusion-controlled catalytic events such as product release from an enzyme active site. The influence of the loss of a single hydrogen bond on protein dynamics in the active site access channel of a glutathione transferase was detected and quantitatively related to a subtle (0.7 kcal/mol) effect on catalysis.

ACKNOWLEDGMENT

The staff of the Vanderbilt Mass Spectrometry Research Center Core Facility and especially Ms. M. Lisa Manier

assisted in optimizing and running the mass spectrometry experiments. Chris Rife provided help in preparing the figures.

SUPPORTING INFORMATION AVAILABLE

Figures S1−S10 describing the fluorescence and CD properties of the native enzyme and Y115F mutant, the peptic peptide map of the protein, and representative kinetic profiles for H−D exchange in peptides covering regions in the protein not discussed in the text. This material is available free of charge via the Internet at http://pubs.acs.org.

REFERENCES

1. Board, P. G., Coggan, M., Chelvanayagam, G., Easteal, S., Jermiin, L. S., Schulte, G. K., Danley, D. E., Hoth, L. R., Griffor, M. C., Kamath, A. V., Rosner, M. H., Chrunyk, B. A., Perregaux, D. E., Gabel, C. A., Geoghegan, K. F., and Pandit, J. (2000) *J. Biol. Chem. 275*, 24798−24806.
2. Armstrong, R. N. (1997) *Chem. Res. Toxicol. 10*, 2−18.
3. Vuilleumier, S. (1997) *J. Bacteriol. 179*, 1431−1441.
4. Hayes, J. D., and Pulford, D. J. (1995) *Crit. Rev. Biochem. Mol. Biol. 30*, 445−600.
5. Pickett, C. B., and Lu, A. Y. (1989) *Annu. Rev. Biochem. 58*, 743−764.
6. Armstrong, R. N. (1998) *Curr. Opin. Chem. Biol. 2*, 618−623.
7. Reinemer, P., Dirr, H. W., Ladenstein, R., Schaffer, J., Gallay, O., and Huber, R. (1991) *EMBO J. 10*, 1997−2005.
8. Ji, X., Zhang, P., Armstrong, R. N., and Gilliland, G. L. (1992) *Biochemistry 31*, 10169−10184.
9. Johnson, W. W., Liu, S., Ji, X., Gilliland, G. L., and Armstrong, R. N. (1993) *J. Biol. Chem. 268*, 11508−11511.
10. Hammes, G. G. (2002) *Biochemistry 41*, 8221−8228.
11. Howard, A. J., Gilliland, G. L., Finzel, B. C., Poulos, T. L., Ohlendorf, D. H., and Salemme, F. R. (1987) *J. Appl. Crystallogr. 20*, 383−387.
12. Ji, X., Johnson, W. W., Sesay, M. A., Dickert, L., Prasad, S. M., Ammon, H. L., Armstrong, R. N., and Gilliland, G. L. (1994) *Biochemistry 33*, 1043−1052.
13. McRee, D. E. (1999) *Practical Protein Crystallography*, 2nd ed., Academic Press, San Diego.
14. Sheldrick, G. M., and Schneider, T. R. (1997) *Methods Enzymol. 277*, 319−343.
15. Berman, H. M., Westbrook, J., Feng, Z., Gilliland, G., Bhat, T. N., Weissig, H., Shindyalov, I. N., and Bourne, P. E. (2000) *Nucleic Acids Res. 28*, 235−242.
16. Wilkins, M. R., Lindskog, I., Gasteiger, E., Bairoch, A., Sanchez, J. C., Hochstrasser, D. F., and Appel, R. D. (1997) *Electrophoresis 18*, 403−408.
17. Engen, J. R., Gmeiner, W. H., Smithgall, T. E., and Smith, D. L. (1999) *Biochemistry 38*, 8926−8935.
18. Mandell, J. G., Falick, A. M., and Komives, E. A. (1998) *Anal. Chem. 70*, 3987−3995.
19. Zhang, Z., Post, C. B., and Smith, D. L. (1996) *Biochemistry 35*, 779−791.
20. Engen, J. R., Smithgall, T. E., Gmeiner, W. H., and Smith, D. L. (1999) *J. Mol. Biol. 287*, 645−656.
21. Resing, K. A., and Ahn, N. G. (1998) *Biochemistry 37*, 463−475.
22. Resing, K. A., Hoofnagle, A. N., and Ahn, N. G. (1999) *J. Am. Soc. Mass Spectrom. 10*, 685−702.
23. Zhang, Z., and Marshall, A. G. (1998) *J. Am. Soc. Mass Spectrom. 9*, 225−233.
24. Zhang, Z., and Smith, D. L. (1993) *Protein Sci. 2*, 522−531.
25. Englander, S. W., and Kallenbach, N. R. (1983) *Q. Rev. Biophys. 16*, 521−655.
26. Englander, S. W., Sosnick, L., Englander, J. J., and Mayne, L. (1996) *Curr. Opin. Struct. Biol. 2*, 18−23.
27. Engen, J. R., and Smith, D. L. (2001) *Anal. Chem. 73*, 256A−265A.
28. Kim, K.-S., and Woodward, C. (1993) *Biochemistry 32*, 9609−9613.
29. Fersht, A. (1999) *Structure and Mechanism in Protein Science*, pp 540−572, Freeman, NewYork.
30. Li, R., and Woodward, C. (1999) *Protein Sci. 8*, 1571−1591.
31. Hoofnagle, A. N., Resing, K. A., Goldsmith, E. J., and Ahn, N. G. (2001) *Proc. Natl. Acad. Sci. U.S.A. 98*, 956−961.
32. Thirumalai, D., and Woodson, S. A. (1996) *Acc. Chem. Res. 29*, 433−439.
33. DeLano, W. L. (2002) The PyMOL Molecular Graphics System (http://www.pymol.org).
34. McCallum, S. A., Hitchens, T. K., Torborg, C., and Rule, G. S. (2000) *Biochemistry 39*, 7343−7356.

BI026776P